Available online at www.sciencedirect.com
SCIENCE DIRECT
Fusion Engineering and Design 81 (2006) 2127–2142
Fusion Engineering and Design
www.elsevier.com/locate/fusengdes

PPCS thermal analysis of bounding accident scenarios using improved computational modelling

R. Pampin *, P.J. Karditsas, M.J. Loughlin, N.P. Taylor

EURATOM/UKAEA Fusion Association, Culham Science Centre, Abingdon, Oxford OX14 3DB, UK

Received 26 October 2005; received in revised form 10 January 2006; accepted 12 January 2006
Available online 28 February 2006

Abstract

Within the framework of the European Power Plant Conceptual Study (PPCS), evaluation of activation inventories and temperature excursions in structures following hypothetical worst-case accident scenarios was performed for the four plant models considered. An improved, three-dimensional computational tool was developed and extensively used to assist in the safety and environmental assessment of the PPCS power plant models. The tool allows for neutron transport, transmutation and thermal analyses to be automated and coupled to the same tokamak geometry. Convenient Monte Carlo and finite elements models of the plants can be easily developed, optimising time and computer resources and removing previous one-dimensional conservatism. The main features of this modelling tool, which for the first time includes an approximation of the divertor, are described here. Results from the bounding accident analyses of the four initial PPCS plant models are reported, including neutron spectra, activation inventories and temperature excursions up to 100 days after the initiation of the accident, at various radial and poloidal locations within the components. They confirm that not even in the bounding scenario significant structural degradation would be expected.

Keywords: PPCS; Power plant; Safety; Bounding accident; Blanket

1. Introduction

The European Power Plant Conceptual Study (PPCS) [1], aimed at providing insight on physics and technology issues of commercial fusion power through the conceptual design and analysis of several power plant models. Economic, safety, environmental, technological and operational performance analyses were conducted, enabling optimisation of the designs and full exploitation of the inherently favourable features of fusion power generation. As part of the safety and environmental assessment of these models carried out at UKAEA-Fusion, two key objectives were pursued: firstly, to ensure that temperature excursions in and radioactive releases from the plant following hypothetical worst-case accident scenarios ("bounding

* Corresponding author. Tel.: +44 1235 466884; fax: +44 1235 466435.
E-mail address: raul.pampin@ukaea.org.uk (R. Pampin).

0920-3796/$ – see front matter © 2006 EURATOM/UKAEA. Published by Elsevier B.V. All rights reserved.
doi:10.1016/j.fusengdes.2006.01.003

accidents") do not challenge the integrity of structures, nor pose a potential radioactive hazard to the population near the site; secondly, to evaluate the active material expected to be generated during the operation and decommissioning of the plant, and ensure that it does not constitute a burden for future generations.

Earlier work during the SEAFP programmes [2], revealed the need for an improved heat transfer modelling and a less conservative evaluation of temperature excursions during bounding accidents in fusion power plants. It was decided to use a commercially available, finite elements (FE) analysis code to perform this task, and to develop a computational tool which automated and coupled the neutron transport, transmutation and thermal analyses to the same plant parameters, geometry, radial build and material composition around the tokamak. This would enable to describe the geometry, simulate the thermal response and define heat transfer and loading conditions both in radial and poloidal dimensions, removing the conservatism of the previous one-dimensional treatment and overall improving the modelling. As a consequence, poloidal as well as radial results on neutron spectra, activation and other radiological information were possible, to be used both in the bounding accident analysis and in the estimation and characterisation of the radioactive waste inventory. Previous studies [3,4] explored this possibility and performed sample calculations to demonstrate the functionality and benefits of this methodology. The tool, named HERCULES, was developed, optimised and extensively used to study the safety and environmental performance of the PPCS conceptual power plants, proving to have extensive capabilities and to serve as a complete and self-consistent code for the nuclear analysis of tokamak fusion devices [5]. Results obtained during the PPCS bounding accident study are presented here.

The PPCS conceptual power plants spanned a wide range of designs, from an advanced ITER to the foreseen ultimately achievable plasma physics and technology. The so-called "near-term" plant models A and B (PMA and PMB) are based on the water-cooled, liquid lithium-lead blanket concept (WCLL), and on the helium-cooled, pebble bed blanket concept (HCPB), respectively. They were designed assuming little extrapolation from current physics and technology, and using relatively well-known materials. The "advanced" plant models C and D (PMC and PMD) are based on the dual coolant, lithium lead blanket concept (DCLL), and on the single coolant, lithium lead blanket concept (SCLL), respectively. They use greater extrapolations from current expertise and more novel materials like silicon or tungsten carbides.

Worst-case accident scenarios assumed instantaneous, total and unmitigated loss of coolant or coolant flow in all structures of the tokamak for a prolonged time, and activation decay as the only heat source during the transient. These highly conservative assumptions present the advantage of a simplified modelling that, whilst not of physical significance for any particular sequence, provides temperature histories that will certainly be upper bounds for any conceivable accident scenario.

2. The HERCULES code

The code system HERCULES provides technological assessment capability for conceptual designs of fusion power plants. It couples the MCNP Monte Carlo neutron transport [6], FISPACT nuclear inventory [7], and COSMOS/M finite element codes [8], to the same tokamak geometry and material compositions. Designed in a modular fashion, each module uses output information produced and processed in the previous one in order to build command input files for the corresponding code, and produces summary output files containing user-specified information. It contains a pre-processor for the generation of the geometry and set up of an MCNP command file. MCNP is called as a subroutine and returns, among other parameters, neutron and photon spectra, primary heating, tritium generation ratio and first wall (FW) loading. The spectra are used to determine decay heat and other activation related parameters by calling the FISPACT code as a subroutine. The overall results, at as many different radial and poloidal positions as desired around the tokamak, are post-processed for obtaining damage rates of the individual materials (structural, armour, multiplier, etc.), helium production, secondary heating (afterheat) and activation inventory time histories, and other parameters of interest in power plant design. A finite elements command file is also produced for its use in COSMOS/M for safety and accident analysis studies.

2.1. Geometry and material compositions

HERCULES geometry is based on the outermost plasma contour. It is described through plasma and machine parameters, and allows for the definition of radial layers and poloidal sectors. One sector within one layer defines a cell, and each cell in a particular layer is made of a homogeneous mixture of the materials in that layer. The code has been designed to be flexible, giving the user full control over the geometry parameters, number of layers and sectors, layer thickness and material compositions and properties. It automatically calculates elemental and isotopic compositions for each cell according to the material volume fractions and the elemental composition of each material.

The parametric equations describing the plasma contour lines in a tokamak following the magnetic field generated by the coils, in radial R and vertical Z co-ordinates are as follows [9]:

$$R = R_\mathrm{p} + a\cos\left(\alpha + \frac{a}{a_\mathrm{p}} C \sin\alpha\right) + \varepsilon a_\mathrm{p} \tag{1}$$

$$Z = ka\sin\alpha \tag{2}$$

where a is the radius, Z the vertical distance from the R-axis, R_p the plasma major radius, a_p the plasma horizontal minor radius, b_p the plasma vertical minor radius, k the plasma elongation ($k = b_\mathrm{p}/a_\mathrm{p}$), C the triangularity and ε_0 is the effective plasma radial shift. Fig. 1 illustrates the parameters in these equations. The neutron transport and FE models closely follow the outermost plasma contour; that is the curve described by the R–Z co-ordinates with the radius set at $a = a_\mathrm{p} - \varepsilon_0$. Eqs. (1) and (2) are used to determine the R and Z co-ordinates that lie on the primary plasma contour at various predetermined values of the poloidal angle α.

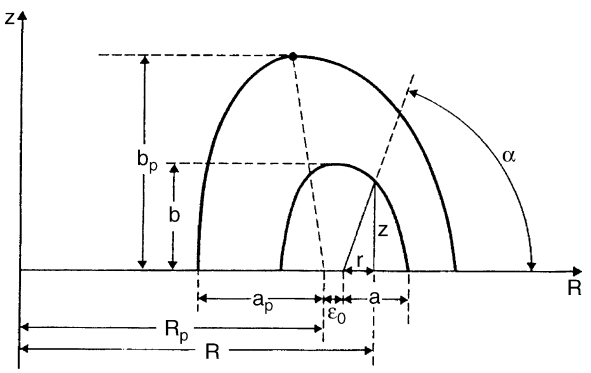

Fig. 1. Diagram of the plasma contour geometry and defining parameters.

The radial build up is divided into inboard and outboard regions: the number of layers must be the same in both, but the thickness and materials may vary. HERCULES allows for any number of layers to be specified but it always assumes three outer ones defining a complete 360° enclosure, and automatically adds gaps between these whose thickness can again be specified as desired. This is the way the radial build of a specific plant model is approximated, illustrated in Fig. 2. A new feature of the system is that it can also accommodate an approximate representation of the divertor. This is located at the bottom of the model, below the plasma, embracing those cells contained in the layers inside the 360° enclosure and a user-specified number of poloidal sectors.

Finally, for purposes of the FE analysis, the cryostat and central solenoid are included. The former consists of a cylindrical structure whose radius, height, thickness and material composition must be specified. It allows for a realistic modelling of the heat rejection by convective exchange with the environment. The solenoid is attached to the outmost inboard layer, and only the internal radius and material composition need to be specified.

2.2. Finite element model

Temperature curves of density, specific heat, thermal conductivity and emissivity must be supplied for each of the materials present in the model. Effective material properties of the layers, as functions of the temperature, are calculated out of them according to the material volume fractions using in-parallel expressions for homogeneous mixtures of materials [10]:

$$k^\mathrm{avg} = \sum_n \upsilon f_n k_n \tag{3}$$

$$\rho^\mathrm{avg} = \sum_n \upsilon f_n \rho_n \tag{4}$$

$$C_p^\mathrm{avg} = \frac{\sum_n \upsilon f_n \rho_n C_{pn}}{\rho^\mathrm{avg}} \tag{5}$$

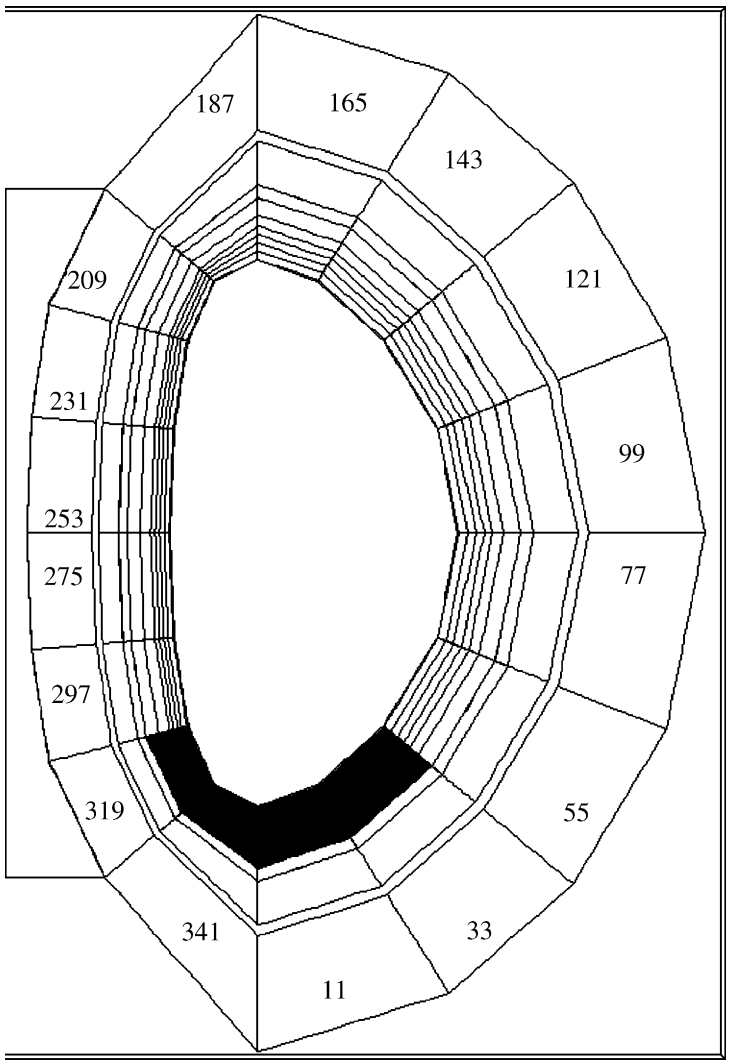

Fig. 2. Example poloidal cross-section of the geometry model showing the poloidal partitioning. The origin of the poloidal angle is placed in the downward vertical semi-axis, and increases counter-clockwise. The dark cells correspond to the divertor, which in this case consists of four poloidal sectors.

where the subscript "n" indicates the n-th material in the cell, "vf" the volume fraction, ρ the density, C_p the specific heat and k is the thermal conductivity. The emissivity of the elements in a layer can be set to that of any of the materials present in its composition.

The partitioning of the model allows specification of different thermal loading depending on radial and poloidal location. Volumetric heating is taken from the FISPACT results on specific decay heat production for each cell. In addition to the decay heat generation and the inherent conduction heat transfer between the elements in the FE grid, radiative heat exchange between the bounding surfaces of the gap/void regions, and between the outer surface and the cryostat structure, are also defined. Finally, the cryostat is allowed to reject heat by convection from the side and top walls to the surroundings, and the groundside can be set at a constant temperature. All these boundary and loading conditions in the FE code can be time and temperature dependent.

3. PPCS plant models

Detailed plant geometry and layout for all four-plant models can be found elsewhere [11], only succinct descriptions are given here. These were conceptually designed following economic criteria, using a systems code to assist in the selection of parameters that minimised the cost of electricity, subject to physics and engineering constraints. The most important machine parameters are listed in Table 1; these were input in HERCULES to generate the neutron transport and FE models.

3.1. Near-term plant models A and B

Both use the low activation Eurofer steel as structural material. PMA is based on a water-cooled, eutectic lithium-lead blanket concept (WCLL) [12]. The radial build consists of first wall, blanket, shield, vacuum vessel (VV) and toroidal field coils (TFC), and the whole plant is cooled by pressurised water. Stagnant LiPb in the blanket provides the necessary neutron multiplication and tritium breeding. The divertor consists of replaceable divertor "cassettes" made of tungsten monoblock targets, Cu alloy heat sink, two Eurofer structural legs and water coolant, plus a fixed shield made of Eurofer and also water-cooled.

PMB is based on a helium-cooled, ceramic pebble bed blanket concept (HCPB) [13]. This concept consists of alternative layers of ceramic Li_4SiO_4 (for tritium breeding) and beryllium (for neutron multiplication) pebble beds, and is helium-cooled. The plant consists of FW, blanket, high and low temperature (HT and LT) shields, manifold, VV and TFC. The LT shield contains $ZrH_{1.7}$ for neutron moderation and shielding. The divertor is a helium-cooled Eurofer structure containing small amounts of tungsten in the plasma-facing components.

Table 1
Plant model machine parameters

Parameter	PMA	PMB	PMC	PMD
Fusion power (GW)	5.50	3.30	3.41	2.46
Major radius (m)	9.8	8.6	7.5	6.1
Aspect ratio	3.0	3.0	3.0	3.0
Elongation	1.9	1.9	2.1	2.1
Triangularity	0.4	0.4	0.7	0.7
SOL thickness (m)	0.15	0.15	0.15	0.15

Both VVs are made of water-cooled conventional steel, and contain small amounts of boron for neutron absorption. Coils are scaled versions of the ITER superconducting magnets.

3.2. Advanced plant models C and D

PMC is based on a dual coolant (LiPb and He), lithium–lead blanket concept (DCLL), whereas PMD is based on a single coolant, lithium–lead blanket concept (SCLL) [11]. They consist of FW, DCLL/SCLL blanket, HT and LT temperature shields, VV and TF coils. The DCLL blanket uses Eurofer as the main structural material, and SiC composite channels for thermal and electrical insulation of the flowing LiPb coolant/breeder. Part of the blanket is also cooled by helium. The SCLL blanket is entirely made of SiC composite and flowing LiPb for cooling and tritium breeding.

PMC has conventional, water-cooled, steel-made HT and LT shields and VV, whereas in PMD these are made of tungsten carbide (WC) and small amounts of SiC composite or steel, and are either LiPb or helium-cooled. The TF coils are again scaled versions of the ITER superconducting coils in both plants. Regarding the divertors, the PMC one consists of a helium-cooled steel structure, and a plasma-facing surface made of steel, helium, tungsten and $W + 1\%La_2O_3$. This last material replaces the TZM alloy used in an earlier version of this divertor design: its removal was decided after preliminary studies demonstrated its inconvenient long-term activation behaviour, as explained in following sections. PMD divertor is a LiPb-cooled, SiC composite support structure for tungsten plasma-facing tiles.

The radial builds of the four plants were approximated into Monte Carlo and FE models using the HERCULES system, within the constraints of this code. The most important characteristics of these models are listed in Table 2. In all of them, 16 poloidal sectors were considered to provide sufficient detail.

4. Calculations and results

4.1. Neutron transport analysis

Plasma sources for the neutron transport calculations had typical thermonuclear plasma features,

Table 2
Characteristics of the Monte Carlo and FE models

	PMA	PMB	PMC	PMD
Radial layers	16	13	21	19
Poloidal sectors	16	16	16	16
Divertor sectors	4	2	4	4
Cryostat				
Height (m)	24.0	22.0	24.0	20.0
Radius (m)	19.0	17.0	18.0	14.0
Thickness (m)	0.1	0.1	0.1	0.1
Solenoid radius (m)	2.0	2.0	2.0	2.0

Table 3
Plasma source parameters for the four PPCS plant models

Parameter	PMA	PMB	PMC	PMD
Major radius (m)	9.80	8.60	7.50	6.10
Ion temperature (keV)	58.0	50.0	36.3	27.3
Elongation	1.7	1.7	1.9	1.9
Triangularity	0.27	0.27	0.47	0.47
Plasma peaking factor	1.7	1.7	2.5	2.5

described using the parameters in Table 3. Neutron energy spectra were calculated with MCNP 4C.3 in all non-void cells of the four models using track length estimation of the particle flux. Spectra were binned using the Vitamin-J 175 energy group structure. Figs. 3–5 show an illustrative sample of the results obtained. Figs. 3 and 4 show the neutron spectra and neutron flux poloidal variation at different radial locations in PMA. Some of the patterns seen in Fig. 4 are found in all four models. In the plasma-facing layer the flux is maximum on the outboard mid-plane segments

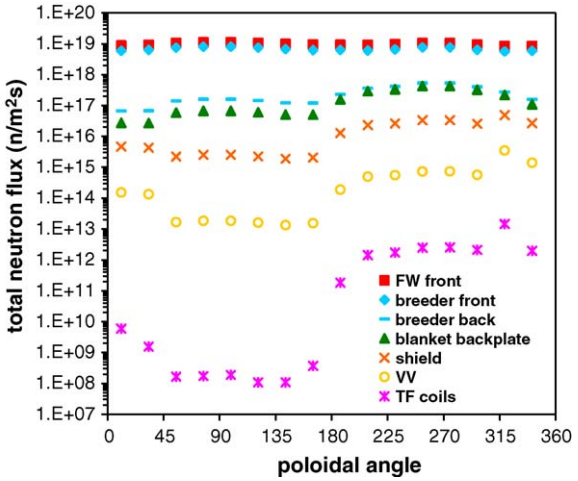

Fig. 4. PPCS plant model A (WCLL blanket) neutron flux poloidal variation (0^0 = vertically downwards) at different radial locations. The two leftmost and two rightmost points in all layers correspond to divertor segments.

and drops off towards the top and bottom of the machine before rising again in the mid-plane inboard sections. This poloidal dependence is expected because the neutron source is centred and peaked in the mid-plane and the flux in this layer is mostly unscattered. This tendency is slightly exaggerated in the advanced plant models due to the higher plasma triangularity (0.47 versus 0.27) and peaking factor (2.5 versus 1.7). The maxima pattern is gradually reversed in inner layers, shifting towards the inboard due to the lower attenuation here (smaller thickness). Also, the further away

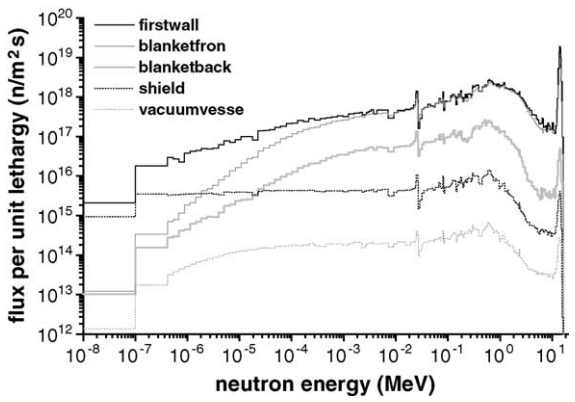

Fig. 3. PPCS model A (WCLL blanket) neutron spectra (flux per unit lethargy) at different radial locations of the inboard mid-plane.

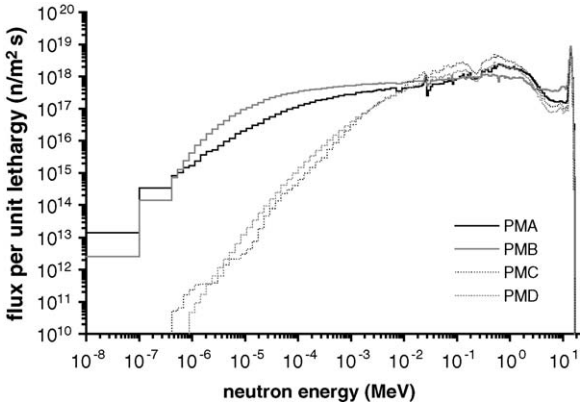

Fig. 5. Comparison of the neutron spectra (flux per unit lethargy) in the breeder region of the four PPCS blanket concepts.

from the plasma, the more exaggerated the poloidal variation is.

In general, divertors do not attenuate the neutron flux as effectively as the blanket. The average mean free path here is longer than that in the breeder materials, and therefore the neutron flux in the structures immediately behind it is larger. In PMA, however, this effect is not as noticeable as in the remaining of the models due to the water coolant, which provides good moderation and attenuation.

Fig. 5 shows the neutron spectra in the inboard mid-plane of the breeder regions of the four plant models; only a qualitative comparison can be made due to the different reactor size and power. The WCLL blanket neutron spectrum is strongly influenced by $(n, 2n)$ reactions in lead. Moderation is not as important as in the HCPB blanket because of the high mass of lead nuclei and the fact that there is only a small quantity of water: in the HCPB design beryllium provides greater moderation, and with the $(n, 2n)$ reactions the resultant spectrum in this blanket is a typical evaporation spectrum in the MeV region, with an extended $1/E$ tail down to low energy. As a consequence, HCPB spectrum is softer than the WCLL and neutron capture reactions are therefore more likely. The DCLL spectrum is again dominated by reactions in lead, but since there is neither water nor beryllium there is even less moderation. These three spectra show common features arising from iron cross-section resonances, due to the presence of steel in all these designs. Finally, the SCLL spectrum is very similar to the DCLL one, only the overall neutron flux is higher and no steel resonances are observed due to the absence of steel and the extensive use of SiC as structural material in this plant model.

4.2. Activation analysis

Activation calculations were performed using the neutron spectra results described previously and the 2001 versions of the inventory code FISPACT and EAF data libraries [14], coupled by the HERCULES system. Irradiation histories were determined for the different components of the plant from available information on the PPCS models and maintenance schemes [11]. The assumed maintenance scheme is shown in Fig. 6. In general terms, it implies service lifetimes of 2.5 years for the divertor, 5 years for the FW and blanket, and

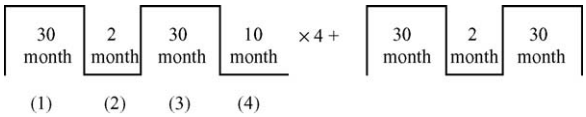

Fig. 6. Proposed PPCS maintenance scheme: (1) 2.5 years at full power operation; (2) two months for divertor replacement (possibly part of the blanket as well, but not considered for this study); (3) another 2.5 years at full power; (4) 10 months for divertor and blanket replacement. The cycle is repeated five times, obviously excluding the last replacement outage. This scheme results in a planned availability of 85.7%.

25 years for the shields, VV and TF coils, but some of the plant models had particular characteristics that altered this scheme. HT shields, for instance, are generally replaced with the blanket, whereas LT shields are permanent components. Also, the SCLL outboard blanket consists of two LiPb "boxes", one of which is replaced, but the other is fixed and remains irradiated during the entire life of the plant. Table 4 shows the irradiation histories of the different components in the four plant models according to the maintenance scheme in Fig. 6.

The results consisted of a huge amount of radiological information, including nuclide inventories, specific activity, specific decay heat and contact dose rate in every cell of each model at a series of predetermined time-steps up to and beyond the transient time, starting at plant shutdown (time zero). These were the basis for subsequent thermal analyses, but also for the estimation and categorisation of the radioactive waste inventories [15]; an illustrative sample is presented here. Time histories and poloidal variation at time zero (i.e. at shutdown) of the specific activity for different radial locations of PMA can be found in Figs. 7 and 8. Some patterns observed in the neutron transport results are repeated here. In general terms, the activation is higher where the neutron flux is higher: in the first, plasma-facing layer of all plant models the activation is maximum at the outboard mid-plane segments, drops off towards the top and bottom, and rises again in the inboard mid-plane. The maxima pattern is reversed in inner layers and shifts towards the inboard where, again, neutron fluxes are higher due to lower attenuation.

Radionuclide decay patterns show no anomalous features. Activity in the steel is dominated by ^{55}Fe ($t_{1/2} = 2.7y$), whose main pathways are ^{56}Fe$(n, 2n)^{55}$Fe

Table 4
PPCS model irradiation histories of the different components

Irradiation history (see Fig. 6)	PMA	PMB	PMC	PMD
(1)	Divertor	Divertor	Divertor	Divertor
(1) + (2) + (3)	FW, WCLL blanket	FW, HCPB blanket, HT shield	FW, DCLL blanket, HT shield	FW, Inboard SCLL blanket, Inboard HT shield, Outboard first box SCLL blanket
Total[a]	Shield, VV, TF coils	LT shield, VV, TF coils	LT shield, VV, TF coils	Outboard second box SCLL blanket, Outboard HT shield, LT shield, VV, TF coils

[a] Meaning: (1) + (2) + (3) + (4) four times, plus (1) + (2) + (3).

for hard, poorly moderated spectra (like those in the FW), and $^{54}Fe(n, \gamma)^{55}Fe$ for soft, moderated spectra (like those in the shields). An interesting feature is the effect that the replacement of the TZM alloy by a mixture of W + 1%La_2O_3 and steel had in the activation of the divertor tiles of PMC and its decay pattern, particularly in the long-term. This is shown in Fig. 9. The removal of the Molybdenum alloy eliminates long-lived activation products like ^{91}Nb ($t_{1/2} = 680y$), ^{93}Mo ($t_{1/2} = 3011y$), ^{93m}Nb ($t_{1/2} = 16.12y$), generated in reactions such as $^{92}Mo(n, pn)^{91}Nb$ and $^{92}Mo(n, \gamma)^{93}Mo(\beta^+)^{93m}Nb$.

4.3. Thermal analysis

The bounding accident hypothesis for the near-term plant models was total loss of coolant for a prolonged time, with no remedial intervention for the duration of the accident sequence. As for the advanced plant models, LiPb is also a coolant and therefore a loss of coolant scenario would eliminate an important contribution to the decay heat generation as well. It was considered that a more conservative assumption was a total loss of cooling flow, in which the LiPb would still be present and contributing to the heat generation, but providing no active heat removal. Therefore total and unmitigated loss of coolant flow for a prolonged time was the assumption used for the analysis of the advanced models.

Following the worst-case methodology, accidents were supposed to occur at the end of the operational life, when decay heat generation is at its maximum.

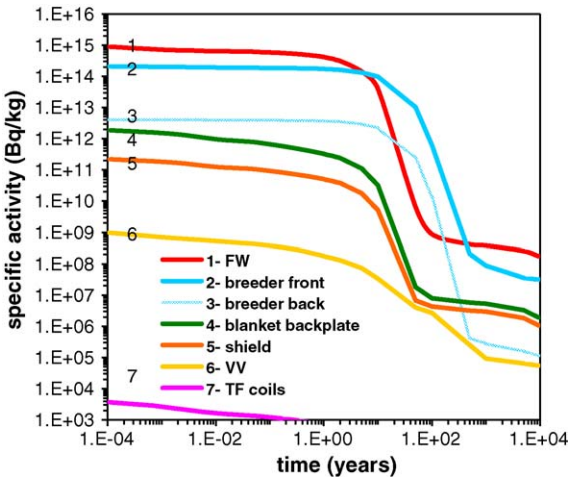

Fig. 7. Time history of specific activity at different radial locations of the outboard mid-plane and at the divertor front of PMA.

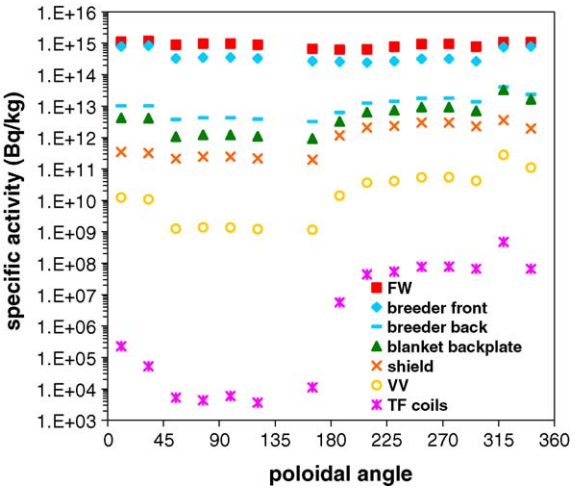

Fig. 8. Poloidal variation (0^0 = vertically downwards) of the specific activity at the time of shutdown, for different radial locations of PMA. The two leftmost and two rightmost points in all layers correspond to divertor segments.

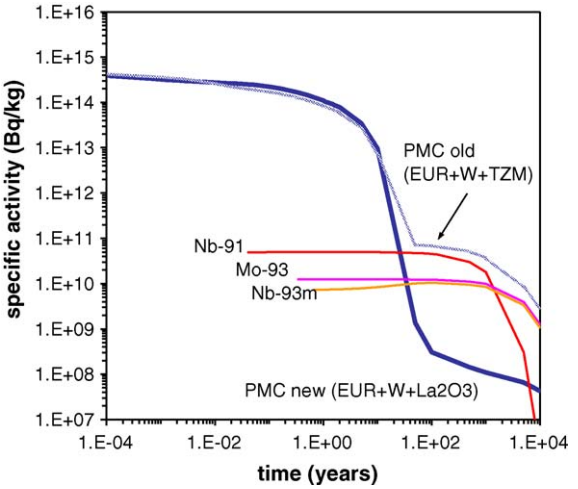

Fig. 9. Comparison of the activity decay pattern in the divertor tiles for the two material compositions: the "old" one meaning a mixture of steel, tungsten and TZM alloy, and the "new" one in which the latter was replaced by a mixture of steel and $W + 1\%La_2O_3$.

Thus the activation calculations described previously provided the necessary decay heat data for the elaboration of volumetric heating time curves. Figs. 10–13 illustrate the trend of the decay heat production in the models during the time of the transient, at the divertor front and different radial positions of the outboard mid-plane. HERCULES was used to prepare suitable time curves to be implemented within the FE models

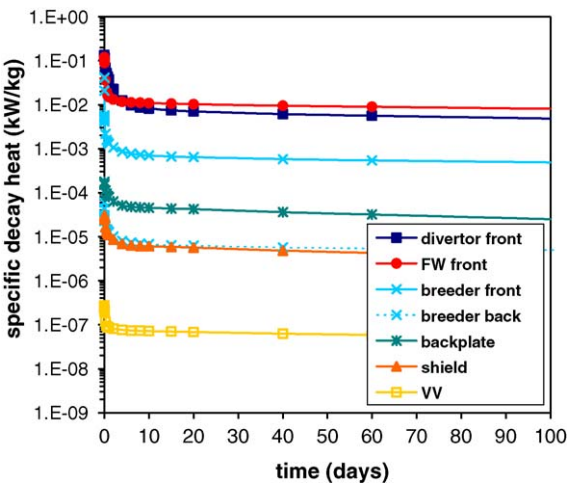

Fig. 10. Specific decay heat production (kW/kg) at the divertor front and at different radial positions of the outboard mid-plane of PMA (WCLL blanket concept).

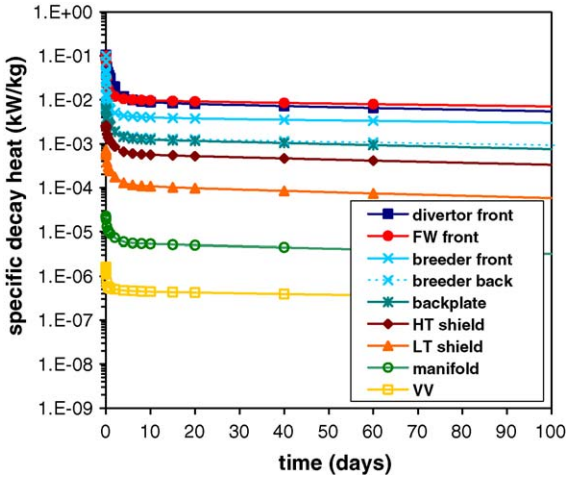

Fig. 11. Specific decay heat production (kW/kg) at the divertor front and at different radial positions of the outboard mid-plane of PMB (HCPB blanket concept).

in COSMOS/M as thermal loads. The thermal transient analyses assumed 400 steps of 6 h each, i.e. a total of 100 days of total loss of cooling flow transient. The initial temperature distribution was assumed as shown in Tables 5 and 6, and was based on design information [11]. The most interesting results can be seen in Figs. 14–18. Figs. 14–17 show the temperature variation with time at the divertor front and different radial

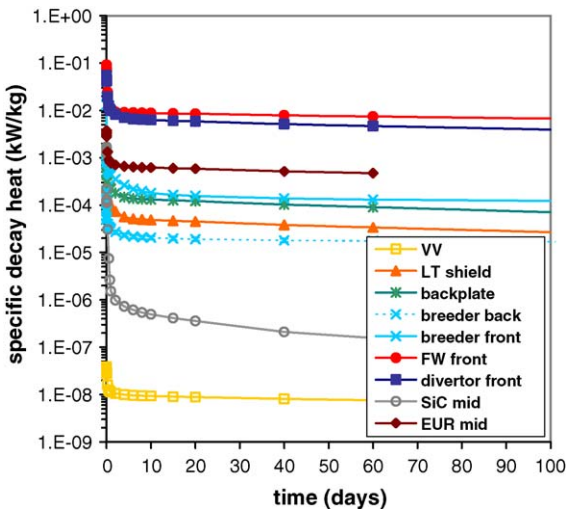

Fig. 12. Specific decay heat production (kW/kg) at the divertor front and at different radial positions of the outboard mid-plane of PMC (DCLL blanket concept).

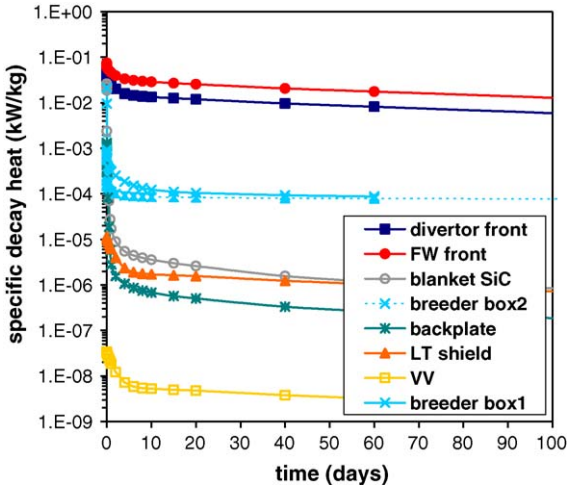

Fig. 13. Specific decay heat production (kW/kg) at the divertor front and at different radial positions of the outboard mid-plane of PMD (SCLL blanket concept).

positions of the outboard mid-plane of all plant models. Fig. 18 shows poloidal profiles and temperature distributions at the mid-plane for different transient times of PMA.

The different characteristics (size, material composition, fusion power), and the consequently different decay heat production, help identify the different thermal response of the plants. A peak occurring within the first 5 days of the transient is observed in PMA. Further analyses [16], revealed that this is due to the presence of the divertor in the model, and a consequence of its approximate modelling. In particular, the divertor model is in direct contact with the blanket and therefore a conduction path is allowed between these two structures. Due to the low conductivity of

Table 5
Initial temperatures of the different PMA and PMB components

Component	Temperature (°C)
PMA	
Cryostat	20
TF coils + solenoid	−173
Vacuum vessel	200
Shield	305
WCLL blanket + FW	305
Divertor	165
PMB	
Cryostat	20
TF coils + solenoid	−173
Vacuum vessel	200
Manifold	200
LT shield	260
HT shield	400
HCPB blanket + FW	400
Divertor	620

Table 6
Initial temperatures of the different PMC and PMD components

Component	Temperature (°C)
PMC	
Cryostat	20
TF coils + solenoid	−173
Vacuum vessel	200
LT shield	300
HT shield	400
Blanket manifold (He)	425
Blanket SiC/steel	500
Blanket LiPb	590
FW	385
Divertor structure	700
Divertor tiles	1000
PMD	
Cryostat	20
TF coils + solenoid	−173
Vacuum vessel	400
LT shield	400
HT shield	900
Blanket SiC	850
Blanket LiPb	900
FW	850
Divertor structure	800
Divertor tiles	1100

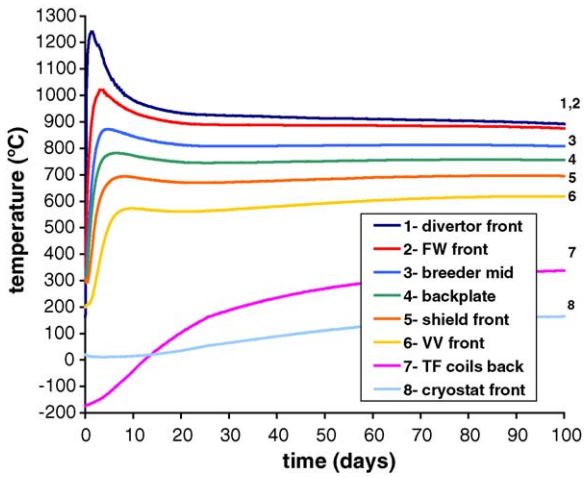

Fig. 14. Temperature histories of the divertor front and of different outboard mid-plane radial locations of PMA.

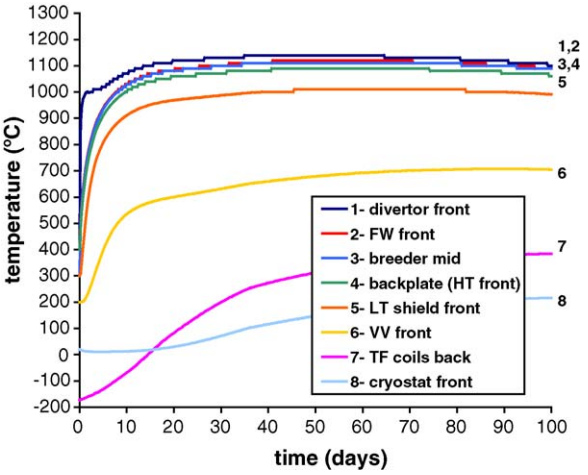

Fig. 15. Temperature histories of the divertor front and of different outboard mid-plane radial locations of PMB.

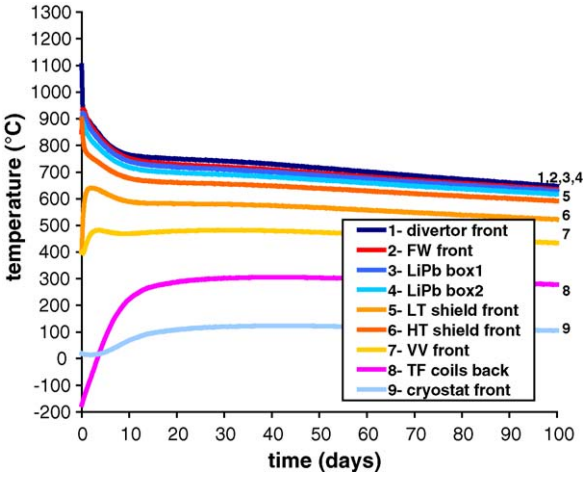

Fig. 17. Temperature histories of the divertor front and of different outboard mid-plane radial locations of PMD.

the WCLL blanket, and to the high early decay heat production in PMA divertor, this structure undergoes a prompt, steep temperature rise. Subsequently, radiative heat exchange within the plasma chamber makes the FW and remaining in-vessel components follow this peak. Since in reality there is no direct contact (i.e. no conduction path) between the divertor and blanket modules, it is expected that the real thermal behaviour of any plant model should be somewhat similar to that of PMA. On the other hand, it is considered that the relatively large size of the divertor in PMA model might be exaggerating this effect. Given the limited divertor modelling capabilities of HERCULES, this feature could only be further explored with a more detailed, purpose-built model of this structure.

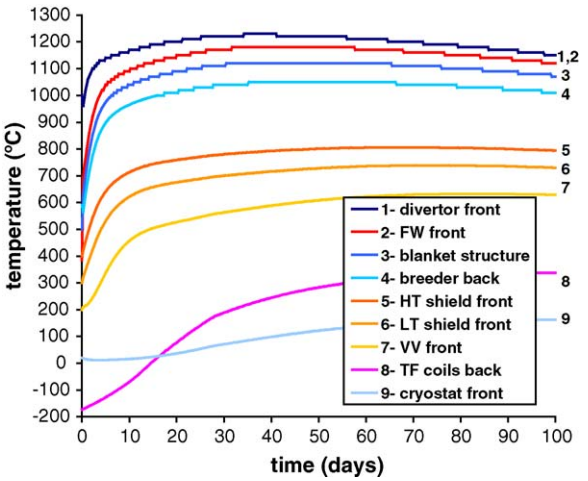

Fig. 16. Temperature histories of the divertor front and of different outboard mid-plane radial locations of PMC.

The provision in the HCPB and DCLL blanket concepts of a helium coolant manifold adds extra obstacles for heat transfer in plant models B and C. When loss of coolant or coolant flow is assumed this layer is an efficient thermal insulator, preventing heat rejection towards outer structures. This creates a noticeable temperature jump between the LT shield and the VV layers in PMB, and between the breeder back and HT shield layers in PMC, precisely where the manifolds are located. This feature can be more clearly seen in Figs. 19 and 20, where steep temperature drops can be observed at radial positions ∼4 m in PMB and ∼3.5 m in PMB and PMC, respectively (locations of the manifolds). Another feature shown in these figures is the similar steep temperature drop in the three gaps between the first four layers in all plant models, consequence of radiation being the only possible heat transfer mechanism here.

Both the DCLL and SCLL blankets consist mostly of LiPb and SiC composite, but PMC also contains a substantial amount of Eurofer as structural material, whose decay heat production during the transient is much higher, as can be seen in Fig. 12. The apparently higher first wall specific decay heat in PMD is due to a thin tungsten armour layer, but it makes only a

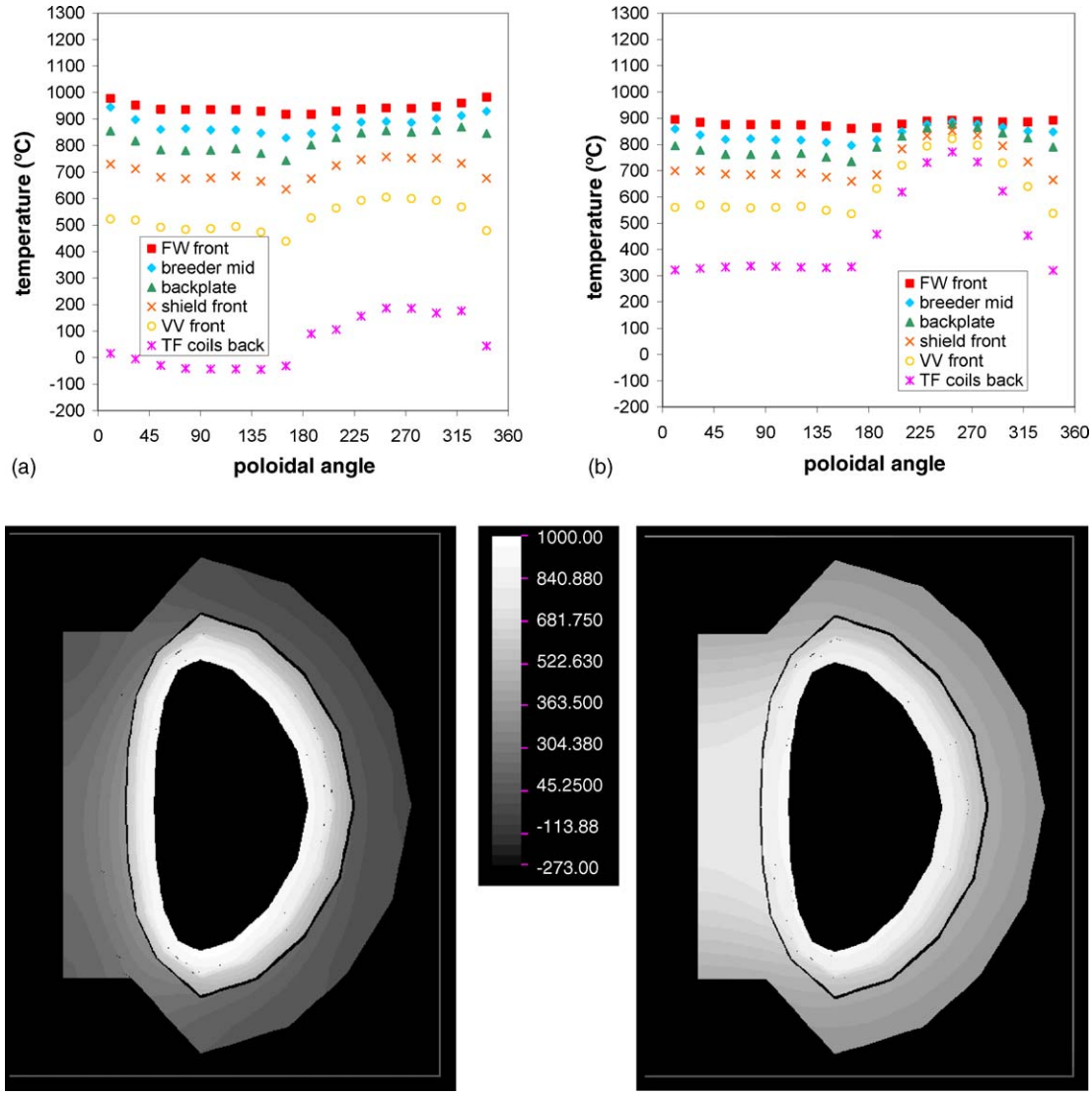

Fig. 18. Poloidal profiles in different layers and temperature distribution in PMA at (a) 10 days and (b) 100 days after initiation of the accident sequence. The two leftmost and two rightmost points in all layers correspond to divertor segments.

small contribution to the overall heat load. Summarising, the better heat conduction in PMD, its lower decay heat load and smaller size results in better heat rejection from the blanket towards outer structures, and thus faster heating of the TF coils and cryostat and much lower in-vessel temperatures than PMC.

Maximum temperatures in PMA, PMB and PMC occur at the inboard mid-plane for all layers, and in the divertor region. This is mainly because heat rejection in the inboard by radiation to the cryostat, where it is removed by convection, is much more difficult given the geometry of the models. In PMA in-vessel components these maxima occur earlier, in the first 5 days, due to the divertor temperature peak. In PMA ex-vessel components and all PMB and PMC components, the maxima occur at later stages of the transient, typically between 80 and 100 days for the first and between 40 and 60 days for the other two. In PMD

Table 7
Bounding accident maximum temperatures at mid-plane and divertor of PMA and PMB

Layer	PMA		PMB	
	Outboard (°C)	Inboard (°C)	Outboard (°C)	Inboard (°C)
FW	1020	1030	1120	1130
Blanket	1020	1030	1120	1130
(HT) shield	697	858	1090	1140
LT shield	–	–	1010	1120
VV	619	836	707	1040
TF coils	429	799	500	990
Cryostat	165		216	
Divertor	1240		1140	

Table 8
Bounding accident maximum temperatures at mid-plane and divertor of PMC and PMD

Layer	PMC		PMD	
	Outboard (°C)	Inboard (°C)	Outboard (°C)	Inboard (°C)
FW	1160	1180	934	935
Blanket	1140	1190	933	934
HT shield	799	1190	900[a]	900[a]
LT shield	731	1180	640	774
VV	625	1150	482	716
TF coils	431	1120	344	692
Cryostat	162		123	
Divertor	1210		1100[a]	

[a] Operational temperatures.

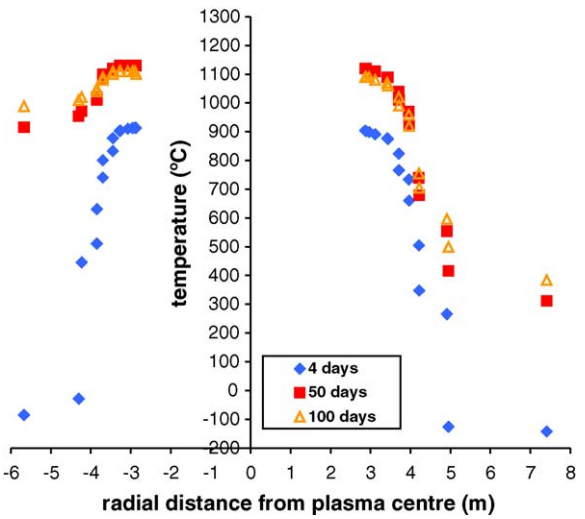

Fig. 19. Radial temperature profiles at the mid-plane of PMB at different times after the initiation of the transient.

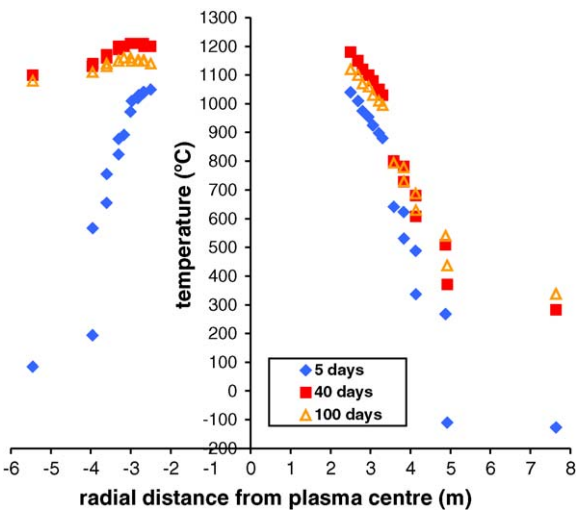

Fig. 20. Radial temperature profiles at the mid-plane of PMC at different times after the initiation of the transient.

all in-vessel temperatures decrease gradually from the very beginning. Inboard maxima are also observed, although much less pronounced. PMD divertor, however, no longer reaches high temperatures in the long term: this is because it consists of LiPb-cooled, SiC composite structure, and therefore its decay heat and heat transfer characteristics are similar to the SCLL blanket (i.e. very good). Tables 7 and 8 summarise the maximum temperatures at the inboard and outboard mid-plane, cryostat and divertor of all plant models.

Inboard maxima are more pronounced in the advanced plant models because of their smaller size. PMC and PMD central solenoids are much closer to the toroidal axis, allowing a very small area for radiative heat exchange with the cryostat compared to the bigger near-term models. In the case of PMD, given its low heat loading, this effect does not produce significantly higher inboard temperatures, but in PMC it makes a difference. This feature, together with the blanket manifold issue and high decay heat production in steel, makes this plant model exhibit the highest temperatures of all four. A generic passive cooling system has been proposed, based on poloidally distributed lead cooling loops located in the vacuum vessel, which would transport heat from the inboard to the outboard by natural circulation of the melted lead in case of overheating due to accidents such as loss of cooling [17]. Regarding the results of this study, it is considered that the effectiveness of this system would be considerably diminished due to the presence of a manifold in plant models such as PMB and PMC.

5. Discussion

Results presented here are part of the outcome of a lengthy and detailed study of bounding accident consequences in the PPCS fusion power plant conceptual designs. The thermal analysis of internally-driven worst-case accident scenarios, which assumed total and unmitigated loss of coolant or coolant flow, has shown that:

- Maximum temperatures are well below the melting point of structural materials. No significant challenge to the integrity of the structures due to decay heat generation is expected in the aftermath of such bounding events.
- Temperature increases at early stages are moderate, indicating that were the accident mitigated within this time scale by some intervention introducing cooling, no safety concerns would arise whatsoever.
- These results hold even for the near-term models: those based on limited extrapolation from current physics and technology expertise.
- For the advanced PPCS models, based on larger extrapolations from current physics and technology, results prove the encouraging potential of fusion power generation regarding safety standards. PMC thermal excursions, however, are in the range of those obtained for the conservative models. The extensive use of steel as structural material, even low activation Eurofer, limits the safety advantages of this concept.

No considerations were made regarding the state of the plant after such a bounding event. The possibility that, if no mitigation is devised, thermo-mechanical stresses could lead to the structural failure and degradation of certain components subject to such temperatures for a prolonged time should be investigated, since in that case the operability of the plant would be compromised.

Optimisation of safe, environmentally friendly and economically viable fusion power plant designs is possible through the study of the bounding accident. Heat transfer obstacles such as manifolds, for instance, have been identified and should be taken into account for future design improvements. A detailed FE analysis of the divertor thermal behaviour, following from the on-going neutron transport and activation analyses, is necessary in order to further investigate some of the features discovered during this modelling. The PPCS programme identified a fifth blanket concept whose potential performance, and selection as one of the European test blanket modules for ITER, triggered the evaluation of this technology for power production. Safety and environmental analyses of the so-called plant model AB, based on a helium-cooled lithium–lead blanket [18], were performed and are reported elsewhere [19]. Within the PPCS framework the HERCULES code was importantly improved and used to perform the calculations presented here. It is now a powerful tool enabling a comprehensive study of the performance of power plant

concepts, not only safety and environmental aspects but also nuclear design.

Regarding the PPCS near-term plant models, comparison is possible between the results presented here and those in [3,4], which also considered WCLL and HCPB-like blankets. In general terms, agreement is reasonable for long-term temperatures considering the early nature of those designs. The main differences are:

- Electric power requirements raised from 1.0 to 1.5 GW, therefore fusion power rose proportionally. A 50% higher power implies a similar increase in the neutron flux, and consequently a roughly similar increase in the activation and decay heat generation.
- Increase in fusion power required changes in geometry and size, in order to limit divertor and wall loading. The effect of this is uncertain because of competing effects. Purely geometrical considerations show that bigger size reduces the heat rejection towards outer structures, but increases the heat rejection from the inboard to the cryostat.
- TF coils initial temperature: the TF coils initial temperature assumed in Refs. [3,4] was 20 °C, and in the present studies this has been assumed to be −173 °C (averaged through TF coils accounting for the cryogenic conditions of the superconductor strands). It is argued that given its size and such low temperature, the TF coils are now very efficient sink for decay heat during loss of cooling. But calculations show that this effect might be offset because of radiative heat exchange from the cryostat to the TF coils at early stages of the transient, when the environment is donating heat to the system through the cryostat instead of rejecting it.
- No divertor model was possible in the FE analysis performed in the earlier work, whereas now it is available and providing new features, such as the early peak in PMA.

Evaluation of upper bounds to the potential radiological consequences to the public, due to postulated radioactive releases arising from these hypothetical accident scenarios, and categorisation of the active waste inventory arising from the operation of the PPCS plants were subsequently undertaken and are reported elsewhere [15,20].

Acknowledgments

The authors would like to thank the PPCS team, and in particular Dr. P. Sardain (EFDA-CSU Garching), Dr. S. Hermsmeyer (FZK Karlsruhe), Dr. P. Norajitra (FZK Karlsruhe) and Dr. L. Giancarli (CEA Saclay), for the valuable information provided for the elaboration of the FE models. This work was funded jointly by the UK Engineering and Physical Sciences Research Council and EURATOM.

References

[1] G. Marbach, I. Cook, D. Maisonnier, The EU power plant conceptual study, Fusion Eng. Des. 63/64 (2002) 1–9.
[2] I. Cook, G. Marbach, L. Di Pace, C. Girard, P. Rocco, N.P. Taylor, Results, conclusions and implications of the SEAFP-2 programme, Fusion Eng. Des. 51/52 (2000) 409–417.
[3] P.J. Karditsas, M.J. Loughlin, Bounding analysis of temperature excursions in accidents using finite elements analysis, Fusion Eng. Des. 58/59 (2001) 1053–1058.
[4] P.J. Karditsas, Temperature excursions in bounding accidents using finite element analysis for a water-cooled lithium lead blanket power plant, in: Proceedings of the 19th IEEE/NPSS SOFE, Atlantic City, January, 2002, pp. 114–117.
[5] R. Pampin, P.J. Karditsas, Fusion power plant performance analysis using the HERCULES code, to appear in Fusion Engineering and Design, in: Proceedings of the seventh ISFNT Conference, Tokyo, May, 2005.
[6] J.F. Briesmeister, MCNP—A general Monte Carlo *N*-particle transport code version 4C, LA-13709-M, 2000.
[7] R.A. Forrest, FISPACT 2001 User Manual, UKAEA FUS 450, March, 2001.
[8] Structural Research and Analysis Corporation, Finite element analysis system COSMOS/M 2.7, Los Angeles 2002.
[9] D.A. D'Ippolitto, Proceedings of the Finite Beta Theory Workshop, Varenna, Italy, 1977, pp. 75–92.
[10] W.E. Han, I. Cook, Temperature transients in reference tokamak reactors following loss of coolant, UKAEA Report AEA-FUS-95, 1991.
[11] D. Maisonnier, I. Cook, P. Sardain, R. Andreani, L. Di Pace, R.A. Forrest, L. Giancarli, S. Hermsmeyer, P. Norajitra, N.P. Taylor, D. Ward for the PPCS team, a conceptual study of fusion power plants: final report of the European Power Plant Conceptual Study (PPCS), EFDA Report, EFDA-RP-RE-5.0, September 2004.
[12] P. Sardain, B. Michel, L. Giancarli, A. Li Puma, Y. Poitevin, J. Szczepanski, et al., Power plant conceptual study—WCLL concept, Fusion Eng. Des. 69 (2003) 769–774.
[13] S. Hermsmeyer, S. Malang, U. Fischer, S. Gordeev, Lay-out of the He-cooled solid breeder model B in the European power plant conceptual study, Fusion Eng. Des. 69 (2003) 281–287.

[14] R.A. Forrest, The European activation file: EAF 2001 cross section library, UKAEA FUS, 451, 2001.
[15] R.A. Forrest, N.P. Taylor, R. Pampin, Categorisation of active material from PPCS model power plants, in: First IAEA Technical Meeting on First Generation of Fusion Power Plants Design and Technology, Vienna, July, 2005.
[16] R. Pampin, P.J. Karditsas, Heat transfer issues in finite elements analysis of bounding accidents in PPCS models, Fusion Sci. Technol. 47 (4) (2005) 1003–1007.
[17] L.V. Boccaccini, S. Gordeev, S. Malang, Passive system for cooling the inboard region in case of a severe accident, Fusion Eng. Des. 63/64 (2002) 251–256.
[18] A. LiPuma, J.L. Berton, B. Branas, L. Boler, J. Doncel, U. Fischer, Breeding blanket design and systems integration for an HCLL fusion power plant, to appear in Fusion Engineering and Design, in: Proceedings of the Seventh ISFNT Conference, Tokyo, May, 2005.
[19] R. Pampin, P.J. Karditsas, N.P. Taylor, Neutron transport and material activation in a power plant based on the HCLL blanket concept, in: First IAEA Technical Meeting on First Generation of Fusion Power Plants Design and Technology, Vienna, July, 2005.
[20] W.E. Han, Consequence calculations for PPCS bounding accidents, Fusion Eng. Des. 75–79 (2005) 1205–1209.